Title
Measurement of collective excitations in VO2 by resonant inelastic x-ray scattering

Journal
Physical Review B, 94(16)

ISSN
2469-9950

Authors
He, Haowei
Gray, AX
Granitzka, P
et al.

Publication Date
2016-10-01

DOI
10.1103/physrevb.94.161119

Peer reviewed

PHYSICAL REVIEW B **94**, 161119(R) (2016)

Measurement of collective excitations in VO_2 by resonant inelastic x-ray scattering

Haowei He,[1] A. X. Gray,[2,3,*] P. Granitzka,[2,4] J. W. Jeong,[5] N. P. Aetukuri,[5] R. Kukreja,[2] Lin Miao,[1,6] S. Alexander Breitweiser,[1] Jinpeng Wu,[2] Y. B. Huang,[7,8] P. Olalde-Velasco,[7] J. Pelliciari,[7] W. F. Schlotter,[9] E. Arenholz,[6] T. Schmitt,[7] M. G. Samant,[5] S. S. P. Parkin,[5] H. A. Dürr,[2] and L. Andrew Wray[1,†]

[1]*Department of Physics, New York University, New York, New York 10003, USA*

[2]*Stanford Institute for Materials and Energy Sciences, SLAC National Accelerator Laboratory, 2575 Sand Hill Road, Menlo Park, California 94025, USA*

[3]*Department of Physics, Temple University, 1925 North 12th Street, Philadelphia, Pennsylvania 19130, USA*

[4]*Van der Waals-Zeeman Institute, University of Amsterdam, NL-1018 XE Amsterdam, The Netherlands*

[5]*IBM Almaden Research Center, San Jose, California 95120, USA*

[6]*Advanced Light Source, Lawrence Berkeley National Laboratory, Berkeley, California 94720, USA*

[7]*Research Department Synchrotron Radiation and Nanotechnology, Paul Scherrer Institut, CH-5232 Villigen PSI, Switzerland*

[8]*Beijing National Laboratory for Condensed Matter Physics, and Institute of Physics, Chinese Academy of Sciences, Beijing 100190, China*

[9]*Linac Coherent Light Source, SLAC National Accelerator Laboratory, Menlo Park, California 94025, USA*

(Received 27 February 2016; revised manuscript received 1 October 2016; published 21 October 2016)

Vanadium dioxide is of broad interest as a spin-$\frac{1}{2}$ electron system that realizes a metal-insulator transition near room temperature, due to a combination of strongly correlated and itinerant electron physics. Here, resonant inelastic x-ray scattering is used to measure the excitation spectrum of charge and spin degrees of freedom at the vanadium L edge under different polarization and temperature conditions, revealing excitations that differ greatly from those seen in optical measurements. These spectra encode the evolution of short-range energetics across the metal-insulator transition, including the low-temperature appearance of a strong candidate for the singlet-triplet excitation of a vanadium dimer.

DOI: 10.1103/PhysRevB.94.161119

Vanadium dioxide is a spin-$\frac{1}{2}$ electron system that undergoes a metal-insulator transition near room temperature [1], and has been the subject of strong interest in both basic and applied research. When cooling through the transition, vanadium atoms pair into strongly hybridized dimers as the the crystal structure changes from a rutile (R phase) to monoclinic ($M1$ phase) [2,3]. The mechanism driving this transition incorporates Peierls splitting of the bonding and antibonding states of the dimer basis [4,5] and represents a fascinating crossover from itinerant to localized behavior in an electron system that is intrinsically poised at the threshold of becoming a Mott insulator [6–11]. A key challenge to establishing a comprehensive understanding of VO_2-based systems is that, though the gapping of symmetric and antisymmetric states within vanadium dimers is of central importance in motivating the metal-to-insulator transition, excitations across these gaps have not yet been experimentally resolved. Here, resonant inelastic x-ray scattering (RIXS) at the vanadium L edge is used to measure the evolution of vanadium site energetics across the transition. Close comparison with a first-principles-based multiplet cluster model is used to identify symmetries within the RIXS spectrum, and reveals a strong candidate for a symmetric-to-antisymmetric excitation that breaks the singlet bond of a low-temperature vanadium dimer.

The orbital character of VO_2 electronic states was first explored by Goodenough [12], and is outlined in Fig. 1(a). The octahedral-like crystal field splits vanadium $3d$ orbitals into π^* (t_{2g}) and σ^* (e_g) manifolds. Electrons in the ground state largely occupy a π^* orbital termed "$d_\parallel$," with lobes that point between neighboring vanadium atoms along the chain axis (c_R axis). When cooling into the low-temperature $M1$ phase [Fig. 1(b)], dimerization of vanadium atoms along the c_R axis splits the $d_\parallel$-derived states into symmetric and antisymmetric manifolds. The $d_\parallel$-derived states are split by the Peierls transition into bonding and antibonding states ($d_\parallel^b$ and $d_\parallel^a$), which are energetically modified and manifest additional density of states (DOS) features (e.g., $d_\parallel^{b*}$) due to local entanglement and correlations [9,10,13].

Elements of strong correlation have been well established in the electronic structure of VO_2 [9,11,14–16], and singlet bonding between dimerized vanadium sites with well-defined $3d^1$ occupation is thought to explain the nonmagnetic nature of the insulating $M1$ phase. However, the excitations that best represent energetic changes upon entering the $M1$ phase, including bonding-antibonding ($d_\parallel^b$-to-$d_\parallel^a$) excitations and the singlet-triplet excitation of vanadium dimers ($d_\parallel^t$), fall within an antisymmetric sector that is not strongly accessed by optical ($Q \sim 0$) spectroscopies. Nonoptical experimental studies of the electronic density of states have largely made use of single-particle spectroscopies in which an electron is added to or removed from a vanadium site, which does not give information about coherent electronic transitions such as the singlet-triplet mode. In the present study, soft x rays provide sufficient momentum transfer along the dimer axis for direct symmetric-to-antisymmetric excitations to appear in the RIXS spectra (see Fig. 3 discussion), making it possible to measure antisymmetric-sector excitations directly as outlined in Fig. 1(b).

High-resolution RIXS measurements were performed at the ADRESS beamline of the Swiss Light Source at the Paul Scherrer Institute [17,18], with a combined energy resolution of better than $\delta E = 90$ meV at an incident energy

*axgray@temple.edu
†lawray@nyu.edu

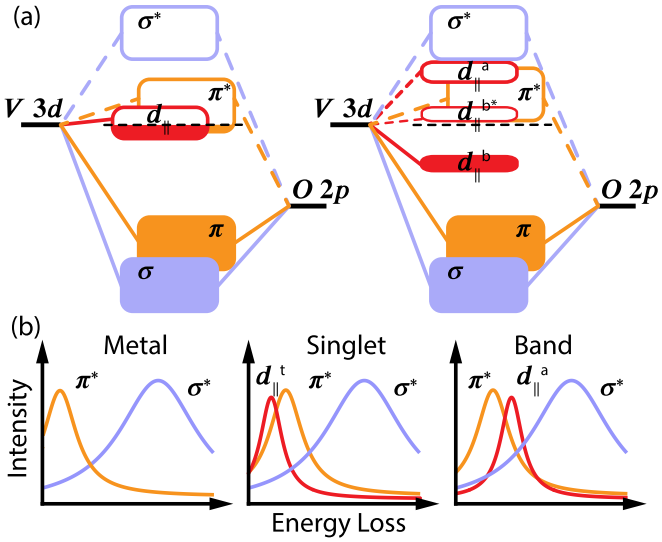

FIG. 1. Orbital symmetries of VO_2 electronic states: (a) Orbital symmetries of electronic states are labeled for (left) the high-temperature metallic state and (right) the low-temperature insulating state, with the Fermi level indicated by a dashed line. The labels $d_{\parallel}^{b*}$ and $d_{\parallel}^{a}$ indicate gapped $d_{\parallel}$-symmetry states expected in the $M1$ phase. (b) Schematics show anticipated RIXS excitations that could be achieved by changing the symmetry of a $d_{\parallel}$ electron. Scenarios are presented for (left) the rutile metal and for hypothetical $M1$ insulating states based on (middle) strongly correlated singlets and (right) itinerant Peierls band physics.

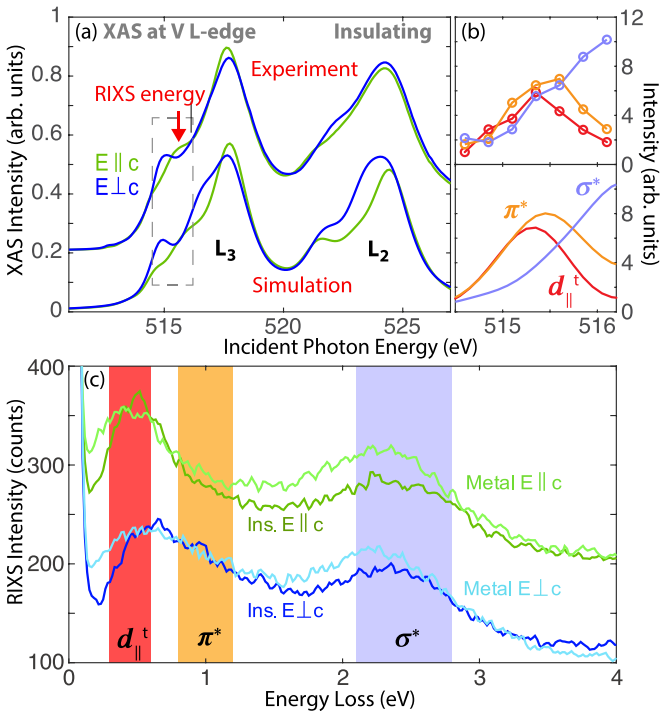

FIG. 2. XAS and RIXS across the metal-insulator transition: (a) Experimental (top) and theoretical (bottom) XAS spectra of $M1$ phase VO_2 are shown for two incident photon polarization conditions. (b) The $M1$ phase $\mathbf{E} \parallel \mathbf{c}_R$ incident energy dependence of highlighted energy loss windows in (c) (top) is compared with simulations for the $d_{\parallel}^{t}$, π^*, and σ^* excitations (bottom). Statistical error bars are slightly smaller than the plotted circles, and simulation curves are weighted to match the integration windows, as described in the SM [20]. (c) RIXS spectra in the insulating and metallic states at temperatures $T = 260$ and 320 K, respectively. The two $\mathbf{E} \parallel \mathbf{c}_R$ curves are upward offset by 100 counts.

of $h\nu = 515.6$ eV. RIXS incident energy dependence was measured with the IRIXS spectrograph at ALS beamline 8, with $\delta E \sim 150$ meV resolution. The linear polarization of the incident photons could be set either perpendicular (σ polarization) or parallel (π polarization) to the scattering plane. This experimental configuration allows one to selectively probe excitations with polarization perpendicular ($\mathbf{E} \perp \mathbf{c}_R$) or near-parallel ($\mathbf{E} \parallel \mathbf{c}_R$) to the rutile c_R axis. Measurements were carried out at temperatures of (insulating) 260 and (metallic) 320 K, with base pressures of better than 5×10^{-11} Torr. The incident photons were maintained at a grazing angle of 15° and RIXS was measured at an acute outgoing angle of 65° with respect to the [001] sample surface (105° at IRIXS). Beam damage was minimized by adopting a new beam spot for each measurement. The high-quality single-crystalline VO_2 film of 10 nm thickness (6 nm for IRIXS) was grown on a TiO_2(001) substrate by pulsed laser deposition, following the procedures described in Ref. [19]. Under these conditions, the metal-insulator transition occurs sharply at $T_{MI} = 295$ K, and the c_R/a_R lattice constant ratio is 0.617 [16,19].

The RIXS and x-ray absorption spectroscopy (XAS) spectral functions are simulated for the experimental scattering geometry by the standard atomic multiplet method, augmented to incorporate two equivalently treated vanadium atoms with interatomic hopping via the $d_{\parallel}$ orbital [see details in the Supplemental Material (SM) [20]]. First-principles calculations estimate the intradimer $d_{\parallel}$ hopping parameter to be more than an order of magnitude larger than interdimer $d_{\parallel}$ hopping [9], making this a good approximated basis for the analysis of low-energy excitations in the $M1$ insulating state.

The vanadium L-edge polarization-dependent XAS spectra of VO_2 in the $M1$ phase are shown in Fig. 2(a) (top). These spectra have been well studied in previous research [19,21], and were used to choose a resonance energy that would provide a good dichroic contrast in the RIXS measurements. High-resolution XAS measurements were carried out using the total electron yield method at the elliptically polarized undulator beamline 4.0.2 of the Advanced Light Source, in the Vector Magnet end station [22], and employed the same experimental geometry as the RIXS measurements. Separate spectral features associated with the L_3 and L_2 core hole symmetries are observed at ~517 and ~524 eV, respectively, each having weak leading edge features followed by a strong high-energy peak. Intensity near the L_3 maximum is greatest with polarization parallel to the axis of vanadium dimerization (c_R axis), while intensity at L_2 is enhanced when polarization is normal to the dimer axis. The atomic multiplet simulation in Fig. 2(a) (bottom) reproduces these characteristics, with a ~0.5 eV discrepancy in some feature energies within the $\mathbf{E} \parallel \mathbf{c}_R$ channel.

Low-energy excitations from 0 to 4 eV are measured by RIXS in Fig. 2(c). Broad features centered at roughly ~0.6 and ~2.3 eV are consistent with the energy gaps

expected for excitation of a $d_\parallel$ electron into the octahedral π^* (t_{2g}) and σ^* (e_g) symmetry state manifolds, and have been labeled accordingly. The incident energy dependence of scattering intensity at each of these features is distinctive, and strongly affirms the attribution of π^* and σ^* symmetry when compared with scattering matrix element calculations [Fig. 2(b)]. Intriguingly, the incident energy dependence of the leading edge of the π^* RIXS feature has a local maximum that is shifted down by ∼0.2 eV in energy, and is consistent with the simulated matrix element of the $d^t_\parallel$ singlet-triplet mode.

Spectral intensity at low temperature has an onset at $E \sim 0.2$ eV, well inside the $\Delta = 0.6$ eV insulating gap of bulk VO_2 [13,23]. This leading edge intensity grows when the sample is heated into the metallic phase, but does not resemble a Drude tail, and unlike the optical gap feature [23–28], the ∼0.6 eV RIXS feature shows no sign of vanishing above the phase transition. These characteristics are consistent with the standard attribution of low-energy L-edge ("direct RIXS" process) features in correlated electron systems to spin excitations and same-atom dd excitations [29], with the delocalized excitations seen by optical spectroscopies manifesting only in the self-energy broadening of these features [30]. The π^* excitation feature has a significant polarization dependence, and has an intensity maximum inside the 0.6 eV bulk insulating gap when measured at low temperature with polarization parallel to the c_R axis. It is also noteworthy that upon cooling into the insulating phase, no feature appears at ∼1.4 eV, the expected energy of a $d^s_\parallel$-to-$d^*_\parallel$ excitation in the itinerant limit (1.4 eV is roughly twice the interdimer $d_\parallel$ hopping parameter [9]).

To understand these spectra, low-energy excited states of the dimerized V_2 atomic multiplet model are used to calculate the RIXS spectral function in Fig. 3, via the Kramers-Heisenberg equation

$$I(E,h\nu) = \sum_f \sum_g \left| \sum_m \frac{\langle f|T^\dagger|m\rangle \langle m|T|g\rangle}{h\nu - E_m + E_g + i\Gamma_m/2} \right|^2 \times \frac{\Gamma_f/2\pi}{\left(E - E_f\right)^2 + (\Gamma_f/2)^2}.$$

Here, the spectral intensity is dependent on both the excitation energy (E) and the incident energy ($h\nu$), which determine the degree of resonance for scattering paths from the ground state g to intermediate core hole states m and the final excited states f, which are broadened by inverse lifetime terms (Γ). All final excited states fall within symmetric ($Q = 0$) or antisymmetric ($Q = \pi$) sectors, and appear with different matrix elements for polarization parallel and perpendicular to the dimer axis [see Figs. 3(a) and 3(b) and Figs. 3(c) and 3(d)]. In the experimental geometry chosen for this study, the momentum (Q) transferred from the scattering event has a component of $Q = 0.26\pi$ along the dimer axis, in units of the inverse distance between nearest-neighbor vanadium atoms. This resulting RIXS spectrum is derived 84% [$\cos(0.26\pi/2)^2 = 0.84$] from the $Q = 0$ final state sector and 16% [$\sin(0.26\pi/2)^2 = 0.16$] from the $Q = \pi$ sector.

All of the symmetry sectors show qualitatively similar RIXS spectra, with prominent peaks at $E \sim 0.8$ eV and $E \sim 2.3$ eV representing transitions from the $d_\parallel$ orbital to nonbonding excited states involving the octahedral π^* (t_{2g}) and σ^* (e_g) manifolds, respectively. The $Q = \pi$ excitation sector differs from the optically accessible $Q = 0$ spectrum in that a singlet-triplet excitation of the dimer is found at $E_t = 0.46$ eV, just 22% reduced from the singlet-triplet gap expected from perturbation theory in the strongly correlated limit ($\frac{4t_\parallel^2}{U} = 4 \times -0.77\ \text{eV}^2/4.0\ \text{eV} = 0.59$ eV). Charge transfer excitations between the vanadium atoms are not seen, as they occur at a higher-energy scale than the plotted range. Calculated spectra for the experimental momentum value [Figs. 3(e) and 3(f)] show the three features outlined in the "singlet" scenario of Fig. 1(b).

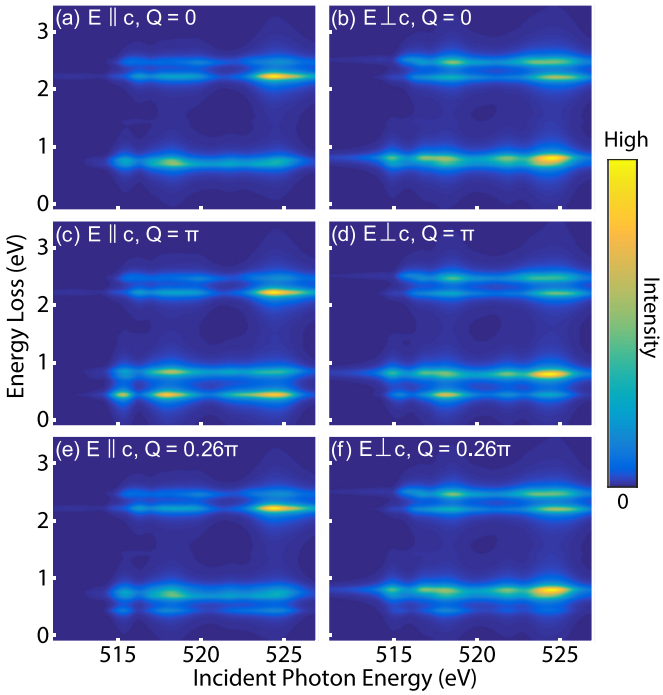

FIG. 3. Simulated RIXS spectra of a vanadium dimer: The RIXS scattering profile is simulated for $\mathbf{E} \parallel \mathbf{c}_R$ polarized incident photons in the high-symmetry (a) $Q = 0$ and (b) $Q = \pi$ sectors, and (c) for a superposition given by the experimental value of $Q = 0.26\pi$. (d)–(f) show corresponding spectra obtained with $\mathbf{E} \perp \mathbf{c}_R$ polarization. Features are plotted with an artificially narrow $\Gamma_f = 0.1$ eV width for visual clarity.

Close comparison between experiment and theory is complicated by the fact that most experimental features appear at energies larger than the bulk VO_2 band gap, and may be significantly broadened due to the rapid decay of multiplet states into delocalized band excitations [30]. Plotting the experimental results over a larger energy range in Fig. 4 reveals that higher-energy line features are qualitatively broader, and sharp line shapes comparable with experimental resolution are only found within the insulating gap. Taking this trend into account, the experimental data under each polarization condition are well fitted by four Lorentzians representing the three low-energy features found in the simulation, as well as one high-energy excitation at 7.2 eV, which can be principally attributed to metal-ligand charge transfer. Feature energies below $E < 4$ eV are lower than nearby peak energies seen

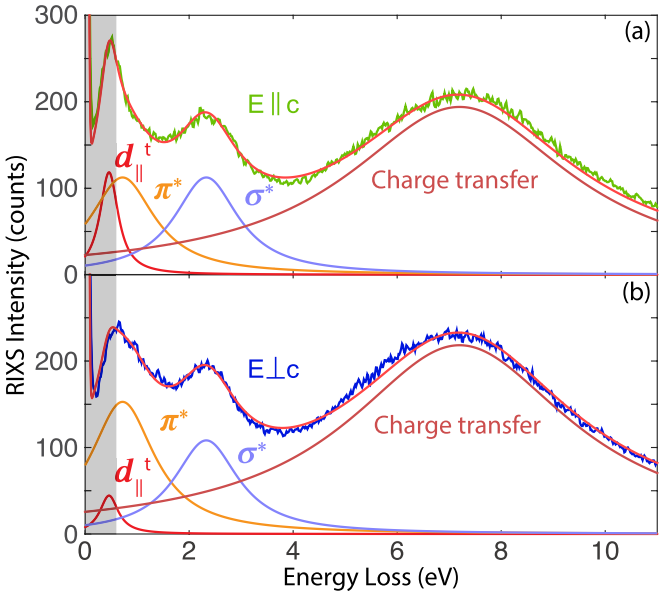

FIG. 4. Polarization dependence and feature attribution: Four-Lorentzian fits of the experimental data measured with incident polarization (a) parallel and (b) perpendicular to the c_R axis. The band gap of bulk VO_2 is shaded in to highlight likely in-gap states. Three low-energy features nominally represent the singlet-triplet mode ($d_{\parallel}^{t}$ at $E_t = 0.46$ eV, width $\Gamma = 0.43$ eV), and dd excitations into nonbonding π^* (t_{2g}) orbitals ($E = 0.72$ eV, $\Gamma = 1.5$ eV) and σ^* (e_g) orbitals ($E = 2.33$ eV, $\Gamma = 1.5$ eV). The broad feature at $E = 7.2$ eV is attributed to metal-ligand charge transfer excitations ($E = 7.2$ eV, $\Gamma = 5.25$ eV). The singlet-triplet excitation constitutes 23% weight of the combined $d_{\parallel}^{t}/\pi^*$ feature when polarization is parallel to the c_R axis, and just 8% under orthogonal polarization.

in the imaginary part of the dielectric constant by optical spectroscopies, and have a strikingly different temperature dependence across the phase transition [23–27]. This is due to differing excitation symmetries in the optical spectrum [28], and to the fact that same-atom dd excitations constitute a dominant low-energy component of L-edge RIXS spectra [29], but are nearly disallowed in optical spectra by angular momentum and reflection selection rules. The direct RIXS excitations of strongly correlated systems with a single electron degree of freedom per atom (e.g., cuprates, vanadates) correspond closely with the difference between orbital site energies set by the crystal field [31], whereas optical excitations represent transitions between band continua.

A particularly dramatic slope is seen from 0.2 to 0.5 eV under $\mathbf{E} \parallel \mathbf{c}_R$ polarization [Fig. 4(a)] and means that, given the above constraints, any good fit for that polarization condition must include a larger component of the narrow singlet-triplet mode. Attribution of this mode to the singlet-triplet dimer-breaking excitation is further supported by the fact that this sharp feature is no longer evident upon heating into the nondimerized metallic phase [Fig. 1(b)], and that no analogous feature is seen in optical ($Q \sim 0$) measurements on analogous thin-film samples [24].

With this feature attribution, we anticipate that future high throughput scattering studies may detailed identify the line-shape properties on the incident energy and energy loss axes that represent the dynamics as atomic positions relax following the breaking of the singlet bond [32]. These dynamics are also likely to cause some incident energy dependence in the RIXS feature energies [33,34]. RIXS spectra obtained at certain incident energies will more accurately represent electronic excitation energetics with unchanged lattice coordinates, while spectra measured at other incident energies will be influenced by a greater degree of lattice relaxation during the core hole resonance state. Unfortunately, our existing incident-energy-dependent data lack the resolution and statistics to facilitate this type of analysis (see curves in the SM [20]).

The identification of a dimer-breaking $d_{\parallel}^{t}$ excitation is further supported by an evaluation of the polarization matrix elements. Within a ± 0.25 eV neighborhood surrounding the RIXS energy, the calculated singlet-triplet scattering cross section accounts for 19% of the intensity in a combined t_{2g} feature under $\mathbf{E} \parallel \mathbf{c}_R$ polarization and 8% of the intensity with $\mathbf{E} \perp \mathbf{c}_R$. These numbers show a good qualitative correspondence with values of 23% and 8%, respectively, from the fit, and substantiate the incident energy analysis in Fig. 2(b).

This triplet excitation is the collective mode that is most fundamentally tied to the metal-to-insulator transition within a wide range of models. The large fitted energy of $E_t = 0.46$ eV is characteristic of strongly correlated exchange energetics, and would not be expected in an itinerant Peierls picture [4]. This experimental E_t value is consistent with the V_2 cluster model and with dynamical mean-field theory (DMFT) predictions [35], but far larger than the value $E_t = 123$ meV obtained in recent quantum Monte Carlo simulations [36]. Comparing with the $\Delta \sim 0.6$ eV bulk optical gap, one finds that the observed mode is also quite similar to the lowest-order expectation of $E_t \gtrsim \frac{2\Delta}{3} \sim 0.4$ eV for a scenario in which the $M1$ phase insulating gap is strongly influenced by magnetic exchange energetics, as suggested in recent DMFT analyses of strongly correlated VO_2 electronic structures [9,10]. Magnetic exchange energetics are less significant for the $M2$ insulating phase, which is not accessible in our sample [20], and future measurements in $M2$ will be useful to obtain a more comprehensive picture of the collective energetics underlying metal-to-insulator transitions in VO_2.

In summary, RIXS has been used to measure the energies of single-particle transitions between the significant orbital manifolds of VO_2. By comparison with a first-principles-derived numerical model, we find a strong correspondence between this spectrum and the electronic states expected in a strongly correlated picture for low-temperature vanadium dimers. Scattering matrix elements are found to enable the experimental measurement of the singlet-triplet excitation that breaks the singlet spin bond of a vanadium dimer. A strong candidate for this key collective mode is identified at $E_t = 0.46$ eV, based on evidence from polarization and temperature dependence, line-shape analysis, and correspondence with energetic expectations in both correlated models and theoretical pictures in which spin entanglement drives the metal-to-insulator transition. These results provide essential ingredients for understanding the gap structure and high-energy landscape underlying the metal-insulator transition of VO_2, and more generally demonstrate the power of the RIXS technique as an incisive probe of correlated energetics in transition-metal compounds.

We are grateful for discussions with G. Kotliar. High-resolution RIXS measurements were performed at the ADRESS beamline of the Swiss Light Source using the SAXES instrument jointly built by Paul Scherrer Institut, Switzerland and Politecnico di Milano, Italy. Work at NYU was supported by the MRSEC Program of the National Science Foundation under Award No. DMR-1420073. A.X.G. acknowledges support from the U.S. Army Research Office, under Grant No. W911NF-15-1-0181 during the writing of this paper. Research at Stanford was supported through the Stanford Institute for Materials and Energy Sciences (SIMES) under Contract No. DE-AC02-76SF00515 and the LCLS by the U.S. Department of Energy, Office of Basic Energy Sciences. The Advanced Light Source is supported by the Director, Office of Science, Office of Basic Energy Sciences, U.S. Department of Energy under Contract No. DE-AC02-05CH11231. J.P. and T.S. acknowledge financial support through the Dysenos AG by Kabelwerke Brugg AG Holding, Fachhochschule Nordwestschweiz, and the Paul Scherrer Institut.

[1] F. J. Morin, Phys. Rev. Lett. **3**, 34 (1959).
[2] B. D. McWhan, M. Marezio, J. P. Remeika, and P. D. Dernier, Phys. Rev. B **10**, 490 (1974).
[3] G. Anderson, Acta Chem. Scand. **10**, 623 (1956).
[4] R. M. Wentzcovitch, W. W. Schulz, and P. B. Allen, Phys. Rev. Lett. **72**, 3389 (1994).
[5] V. Eyert, Ann. Phys. **11**, 650 (2002).
[6] A. Zylbersztejn and N. F. Mott, Phys. Rev. B **11**, 4383 (1975).
[7] C. Sommers and S. Doniach, Solid State Commun. **28**, 133 (1978).
[8] T. M. Rice, H. Launois, and J. P. Pouget, Phys. Rev. Lett. **73**, 3042 (1994).
[9] S. Biermann, A. Poteryaev, A. I. Lichtenstein, and A. Georges, Phys. Rev. Lett. **94**, 026404 (2005).
[10] W. H. Brito, M. C. O. Aguiar, K. Haule, and G. Kotliar, Phys. Rev. Lett. **117**, 056402 (2016).
[11] C. Weber, D. D. O'Regan, N. D. M. Hine, M. C. Payne, G. Kotliar, and P. B. Littlewood, Phys. Rev. Lett. **108**, 256402 (2012).
[12] J. B. Goodenough, J. Solid State Chem. **3**, 490 (1971).
[13] T. C. Koethe, Z. Hu, M. W. Haverkort, C. Schüßler-Langeheine, F. Venturini, N. B. Brookes, O. Tjernberg, W. Reichelt, H. H. Hsieh, H.-J. Lin, C. T. Chen, and L. H. Tjeng, Phys. Rev. Lett. **97**, 116402 (2006).
[14] A. S. Belozerov, M. A. Korotin, and V. I. Anisimov, and A. I. Poteryaev, Phys. Rev. B **85**, 045109 (2012).
[15] Z. Zhu and U. Schwingenschlogl, Phys. Rev. B **86**, 075149 (2012).
[16] A. X. Gray, J. Jeong, N. P. Aetukuri, P. Granitzka, Z. Chen, R. Kukreja, D. Higley, T. Chase, A. H. Reid, H. Ohldag, M. A. Marcus, A. Scholl, A. T. Young, A. Doran, C. A. Jenkins, P. Shafer, E. Arenholz, M. G. Samant, S. S. P. Parkin, and H. A. Dürr, Phys. Rev. Lett. **116**, 116403 (2016).
[17] V. N. Strocov *et al.*, J. Synchrotron Radiat. **17**, 631 (2010).
[18] G. Ghiringhelli *et al.*, Rev. Sci. Instrum. **77**, 113108 (2006).
[19] N. B. Aetukuri *et al.*, Nat. Phys. **9**, 661 (2013).
[20] See Supplemental Material at http://link.aps.org/supplemental/10.1103/PhysRevB.94.161119 for additional experimental details and a summary of the modeling parameters.
[21] M. W. Haverkort, Z. Hu, A. Tanaka, W. Reichelt, S. V. Streltsov, M. A. Korotin, V. I. Anisimov, H. H. Hsieh, H.-J. Lin, C. T. Chen, and D. I. Khomskii, and L. H. Tjeng, Phys. Rev. Lett. **95**, 196404 (2005),
[22] A. T. Young *et al.*, Surf. Rev. Lett. **9**, 549 (2002).
[23] H. W. Verleur, A. S. Barker, and C. N. Berglund, Phys. Rev. **172**, 788 (1968).
[24] K. Okazaki, S. Sugai, Y. Muraoka, and Z. Hiroi, Phys. Rev. B **73**, 165116 (2006).
[25] M. Nazari, Y. Zhao, V. V. Kuryatkov, Z. Y. Fan, A. A. Bernussi, and M. Holtz, Phys. Rev. B **87**, 035142 (2013)
[26] M. M. Qazilbash, A. A. Schafgans, K. S. Burch, S. J. Yun, B. G. Chae, B. J. Kim, H. T. Kim, and D. N. Basov, Phys. Rev. B **77**, 115121 (2008).
[27] J. B. Kana Kana, J. M. Ndjaka, G. Vignaud, A. Gibaud, and M. Maaza, Opt. Commun. **284**, 807 (2011).
[28] J. M. Tomczak and S. Biermann, Phys. Rev. B **80**, 085117 (2009).
[29] L. J. P. Ament *et al.*, Rev. Mod. Phys. **83**, 705 (2011).
[30] L. A. Wray *et al.*, Front. Phys. **3**, 32 (2015).
[31] M. M. Sala *et al.*, New J. Phys. **13**, 043026 (2011).
[32] L. A. Wray, S.-W. Huang, Y. Xia, M. Z. Hasan, C. Mathy, H. Eisaki, Z. Hussain, and Y.-D. Chuang, Phys. Rev. B **91**, 035131 (2015).
[33] J. N. Hancock, G. Chabot-Couture, and M. Greven, New J. Phys. **12**, 033001 (2010).
[34] J. J. Lee, B. Moritz, W. S. Lee, M. Yi, C. J. Jia, A. P. Sorini, K. Kudo, Y. Koike, K. J. Zhou, C. Monney, V. Strocov, L. Patthey, T. Schmitt, T. P. Devereaux, and Z. X. Shen, Phys. Rev. B **89**, 041104(R) (2014).
[35] G. Kotliar (private communication).
[36] H. Zheng and L. K. Wagner, Phys. Rev. Lett. **114**, 176401 (2015).